Impact of Thermal Cutoff Modifications on Thermodynamics and Net-Baryon Number Fluctuations in the (P)NJL Model: An RG-Consistency Perspective*

Jie Tang (唐杰) Fan Lin (林凡)† Xinyang Wang (王昕杨)‡

Center for Fundamental Physics, School of Mechanics and Physics, Anhui University of Science and Technology, Huainan, Anhui 232001, People's Republic of China

Abstract: We investigate the thermodynamic properties, chiral phase transitions, and net-baryon-number fluctuations in the two-flavor NJL and PNJL models from the perspective of renormalization group (RG) consistency. In effective field theories with a fixed vacuum cutoff Λ_0, finite-temperature medium effects require high-momentum thermal fluctuations above the Matsubara scale ($\Lambda \gtrsim \pi T$) to be adequately accounted for. In practice, this is achieved by using unrestricted thermal momentum integration ($\Lambda_T = k\Lambda_0 \to \infty$). This treatment partially restores RG consistency and ensures proper convergence toward the Stefan–Boltzmann limit at high temperatures. To systematically assess the regularization artifacts arising from finite thermal cutoffs commonly used in the literature, we introduce the truncation factor k not as an additional free model parameter but as an exploratory diagnostic tool for mapping the phase-space transition between the strictly truncated scheme ($k = 1$) and the unregularized thermal continuum ($k \to \infty$). Our analysis shows that, although taking $k \to \infty$ smoothly resolves violations of causality ($v_s^2 > 1$) in the standard NJL model by constraining the speed of sound to the conformal limit 1/3, the PNJL model exhibits a more intricate, nonmonotonic sensitivity to k. In this case, intermediate truncation scales ($k \approx 3$) produce a temporary overshoot of the conformal bound due to the nontrivial competition between Polyakov-loop confinement dynamics and thermal integration boundaries. Furthermore, while the unregularized ($k \to \infty$) PNJL framework substantially improves the qualitative description of net-baryon-number fluctuations ($\kappa\sigma^2$) relative to lattice QCD data at vanishing chemical potential, the pronounced amplification of fluctuation extrema at high baryon density underscores the model's sensitivity to high-momentum thermal modes. This work clarifies the role of thermal regularization and provides critical insights into the interplay between confinement dynamics and thermal boundaries in effective chiral theories.

Keywords: (P)NJL model, Renormalization group consistent, Thermal cutoff

DOI: **CSTR:**

CPC Accepted

I. INTRODUCTION

The properties of Quantum Chromodynamics (QCD) matter at finite temperature and baryon density constitute one of the central frontiers in high-energy physics. Theoretical studies predict that QCD matter undergoes phase transitions as the temperature and baryon density increase [1−3]. Current theoretical understanding suggests that the chiral phase transition of QCD proceeds as a smooth crossover at low baryon chemical potential (μ_B), whereas it is expected to become a first-order phase transition at larger μ_B. The endpoint separating these two regimes is commonly referred to as the QCD critical point [4, 5]. Near this critical point, long-range correlations develop, and the correlation length of the system increases significantly [6]. Consequently, event-by-event fluctuations of conserved charges are strongly enhanced [7]. In particular, the cumulants of the net-proton number, which are sensitive to the correlation length, are expected to exhibit characteristic critical behavior and may even diverge in the vicinity of the critical point. Over the past decade, extensive experimental efforts have therefore fo-

Received 18 May 2026; Accepted 29 October 2026

* The work of F. L. was supported by the National Natural Science Foundation of China (NSFC) under Grant No. 12547138 and by the Scientific Research Foundation for Introduced Talents of Anhui University of Science and Technology (AUST) under Grant No. 2025yjrc0143. X. W. was supported by the NSFC under Grants No. 12675170 and No. 12635010 and by AUST under Grant No. YJ20240001

† E-mail: linfan@aust.edu.cn

‡ E-mail: wangxy@aust.edu.cn

Content from this work may be used under the terms of the Creative Commons Attribution 3.0 licence. Any further distribution of this work must maintain attribution to the author(s) and the title of the work, journal citation and DOI. Article funded by SCOAP[3] and published under licence by Chinese Physical Society and the Institute of High Energy Physics of the Chinese Academy of Sciences and the Institute of Modern Physics of the Chinese Academy of Sciences and IOP Publishing Ltd

cused on searching for signatures of the QCD critical point through measurements of fluctuation observables [8, 9]. These fluctuation observables, or equivalently the corresponding susceptibilities, provide an important experimental probe for mapping the structure of the QCD phase diagram. Recent experimental results [10, 11] report significant signals in the ratio C_4/C_2, which may serve as a characteristic indicator of nontrivial structures in the QCD phase diagram.

In the theoretical context, the infrared behavior of QCD is difficult to address because of its intrinsically non-perturbative nature. Lattice QCD provides a powerful first-principles approach; however, it still suffers from the well-known sign problem at finite baryon density. Consequently, effective field theories remain among the most practical and reliable approaches for exploring non-perturbative aspects of QCD. Among these approaches, the Nambu–Jona–Lasinio (NJL) model [12−15] is one of the most widely used low-energy effective theories of QCD, particularly for studying spontaneous chiral symmetry breaking and its restoration at finite temperature and density [16−18]. To incorporate aspects of gluon dynamics, the Polyakov loop is introduced, leading to the so-called Polyakov–Nambu–Jona–Lasinio (PNJL) model [19]. This extension enables the simultaneous investigation of the chiral phase transition and the confinement/deconfinement transition within an effective field theory framework [1, 20, 21]. Nevertheless, as four-fermion interaction theories, both the NJL and PNJL models are non-renormalizable. As a result, the choice of regularization scheme becomes an essential component of the model and remains under active discussion. In practice, various cutoff schemes are employed to regularize the vacuum contribution, including sharp or smooth cutoffs in three-momentum or four-momentum space [14, 15]. For the thermal contribution, however, whether regularization is necessary remains debated; detailed discussions can be found in Refs. [22−25]. Imposing a strict cutoff Λ_0 on the thermal sector ($k=1$) severely restricts the accessible thermal phase space, inducing severe unphysical artifacts such as causality violations ($v_s^2>1$) and suppression of the high-temperature Stefan-Boltzmann limit. Conversely, leaving the thermal sector unregularized ($k\to\infty$) while maintaining the vacuum sector truncated at Λ_0 has been widely adopted in the literature to ensure thermodynamic consistency and correct asymptotic scaling, although the detailed sensitivity of fluctuation observables to this thermal truncation boundary remains incompletely understood.

Recently, the concept of renormalization group (RG) consistency has provided fundamental guidance for low-energy effective theories (LEFTs) at finite temperature and density [26, 27]. In an exact RG-consistent framework, the full quantum effective action in the infrared ($\Gamma_{k=0}$) is required to be independent of the initial ultraviolet cutoff scale, whether denoted by Λ or Λ'.

$$\lim_{\Lambda\to+\infty}\Lambda\frac{d\Gamma}{d\Lambda}=0, \tag{1}$$

This procedure ensures that RG flows initialized at different UV scales flow to the same physical result in vacuum, provided that the bare couplings are properly tuned along the RG trajectory [27, 28]. In a thermal medium, however, the characteristic momentum scale of thermal fluctuations is governed by Matsubara modes with $p\sim\pi T$. Consequently, the ultraviolet cutoff must satisfy $\Lambda\geq\pi T$ to adequately capture thermal excitations; otherwise, thermal fluctuations above Λ cannot be included, leading to discrepancies in the infrared medium properties [28].

In low-energy effective models such as the NJL model, achieving an ideal functional RG improvement, namely continuously increasing the UV cutoff Λ while simultaneously evolving the bare parameters to keep all vacuum observables invariant, presents considerable theoretical and practical challenges because of non-renormalizability. As an alternative, a widely adopted practical realization is to keep the vacuum cutoff at its phenomenologically fixed value, $\Lambda_0\simeq 650\,\mathrm{MeV}$, while extending or completely removing the cutoff in the thermal sector ($\Lambda_T=k\Lambda_0\to\infty$). As demonstrated in Ref. [28], this treatment partially restores RG consistency by fully incorporating all thermal fluctuations above the scale Λ_0 without distorting the calibrated low-energy vacuum physics. In this context, the parameter k should not be interpreted as an additional free model parameter to be tuned phenomenologically. Rather, k serves as a systematic truncation factor that allows one to explore the continuous evolution from a strictly restricted thermal phase space ($k=1$) to the unregularized thermal limit ($k\to\infty$), thereby directly evaluating the regularization artifacts reported in the literature [23].

Furthermore, when this framework is extended to include gluonic degrees of freedom via the Polyakov loop (PNJL model), the interplay between the thermal momentum boundary and the confining background gauge field becomes highly nontrivial. Whereas taking $k\to\infty$ smoothly restores compliance with the conformal bound ($v_s^2\leq 1/3$) and ensures convergence toward the Stefan-Boltzmann limit in the baseline NJL model, the inclusion of the Polyakov-loop effective potential induces a non-monotonic dependence of the speed of sound on k, with intermediate values ($k\approx 3$) temporarily violating the conformal bound. This behavior reveals an intrinsic competition between confinement dynamics and the thermal integration boundary.

In this study, we systematically analyze the impact of thermal cutoff modifications on the chiral phase transition, thermodynamic properties, and net-baryon number

CPC Accepted

fluctuations within both the NJL and PNJL frameworks from an RG-consistency perspective. By analyzing the parametric sensitivity to the truncation factor k up to the asymptotic $k \to \infty$ limit, we delineate the range of physical validity of thermal regularization prescriptions and compare the calculated baryon number kurtosis with recent lattice QCD data and experimental measurements.

The paper is organized as follows. In Sec. II, we review the theoretical framework of the RG(P)NJL model and discuss the associated regularization schemes. In Sec. III, we analyze the chiral phase transition within this framework. In Sec. IV, we present results for thermodynamic quantities and baryon number fluctuations. Finally, Sec. V provides a summary and an outlook for future research.

II. FORMALISM

In this section, we introduce the two-flavor, RG-improved NJL/PNJL models, which are among the most widely used low-energy effective theories of QCD.

The Lagrangian density of the two-flavor NJL model is given by

$$\mathcal{L}_{\rm NJL} = \bar{\psi}\left(i\gamma^{\mu}\partial_{\mu} - \hat{m}\right)\psi + G_S\left[(\bar{\psi}\psi)^2 + \left(\bar{\psi}i\gamma^5\boldsymbol{\tau}\psi\right)^2\right], \quad (2)$$

where $\psi = (u,d)^{\rm T}$ denotes the two-flavor quark field, and $\hat{m} = {\rm diag}(m_u, m_d)$ is the current-quark mass matrix. For simplicity, isospin symmetry is assumed, $m_u = m_d = m$. The Pauli matrices $\boldsymbol{\tau} = (\tau^1, \tau^2, \tau^3)$ act in flavor space. The coupling constant G_S characterizes the interaction strength in the scalar and pseudoscalar channels.

Within the mean-field approximation, quantum fluctuations around the condensates are neglected, and the four-fermion interactions are linearized as

$$\begin{aligned}(\bar{\psi}\psi)^2 &= 2\langle\bar{\psi}\psi\rangle\bar{\psi}\psi - \langle\bar{\psi}\psi\rangle^2,\\ (\bar{\psi}i\gamma^5\boldsymbol{\tau}\psi)^2 &= 2\langle\bar{\psi}i\gamma^5\boldsymbol{\tau}\psi\rangle\bar{\psi}i\gamma^5\boldsymbol{\tau}\psi - \langle\bar{\psi}i\gamma^5\boldsymbol{\tau}\psi\rangle^2.\end{aligned} \quad (3)$$

Here, $\langle\bar{\psi}\psi\rangle$ and $\langle\bar{\psi}i\gamma^5\boldsymbol{\tau}\psi\rangle$ denote the chiral and pseudoscalar condensates, respectively. In the absence of an axial chemical potential μ_5, the pseudoscalar condensate vanishes, $\langle\bar{\psi}i\gamma^5\boldsymbol{\tau}\psi\rangle = 0$. The Lagrangian density then reduces to

$$\begin{aligned}\mathcal{L}_{\rm NJL} &= \bar{\psi}\left(i\gamma^{\mu}\partial_{\mu} - \hat{m} + 2G_S\langle\bar{\psi}\psi\rangle\right)\psi - G_S\langle\bar{\psi}\psi\rangle^2\\ &= \bar{\psi}\left(i\gamma^{\mu}\partial_{\mu} - M\right)\psi - \frac{(M-m)^2}{4G_S},\end{aligned} \quad (4)$$

where we have introduced the constituent quark mass $M = m - 2G_S\langle\bar{\psi}\psi\rangle$.

The constituent quark mass is determined self-consistently from the thermodynamic potential after finite-temperature and finite-chemical-potential effects are taken into account. Following standard procedures [14, 15, 29], the one-loop grand thermodynamic potential at finite temperature T and quark chemical potential μ can be written as

$$\begin{aligned}\Omega_{\rm NJL} = \frac{(M-m)^2}{4G_S} - 2N_cN_f\int\frac{d^3p}{(2\pi)^3}\\ \times\left[E + T\ln\left(1+e^{-\beta(E-\mu)}\right) + T\ln\left(1+e^{-\beta(E+\mu)}\right)\right],\end{aligned} \quad (5)$$

where $\beta = 1/T$, and $E = \sqrt{p^2+M^2}$ denotes the single-particle dispersion relation of the constituent quark. The physical value of the constituent quark mass is obtained by minimizing the thermodynamic potential, which is equivalent to solving the gap equation

$$\frac{d\Omega_{\rm NJL}}{dM} = 0. \quad (6)$$

However, this equation cannot be solved without further specification because the NJL model is non-renormalizable and the momentum integral is ultraviolet divergent. Therefore, an appropriate regularization scheme must be introduced before numerical evaluation.

In practice, the ultraviolet divergence in the vacuum contribution is typically treated by introducing a momentum cutoff. A common choice is the three-momentum regularization scheme. For instance, in the hard-cutoff scheme, the upper limit of the momentum integral is replaced by a finite cutoff Λ; that is, the integration range is restricted from $[0,\infty)$ to $[0,\Lambda]$. By contrast, for the thermal contribution to the thermodynamic potential, whether a similar cutoff should be imposed remains under debate. As discussed in Ref. [23], applying the cutoff to the finite (thermal) part of the integral may lead to inconsistencies, and different prescriptions can yield qualitatively different results. Recently, the implementation of RG consistency in effective theories has provided a more systematic framework for addressing this issue and further clarifying the role of the cutoff in both vacuum and thermal contributions.

As shown in Ref. [28], imposing the RG consistency condition in Eq. (1) on the NJL model modifies the regularization procedure. In particular, an additional cutoff scale is introduced for the thermal contribution, which can be parameterized as $\Lambda_T = k\Lambda_0$. In general, for a medium with temperature or chemical potential exceeding the vacuum cutoff scale Λ_0, contributions from higher-momentum modes become relevant. This implies that the parameter k should satisfy $k \geq 1$, with its precise value determined by the physical conditions under consideration. Here, k acts as an exploratory truncation parameter that maps the phase-space transition between a highly restric-

CPC Accepted

ted thermal medium ($k=1$) and an unregularized thermal continuum ($k\to\infty$). We emphasize that k is not introduced as an additional adjustable parameter for fitting empirical data, but rather as a diagnostic scale factor for systematically investigating how finite thermal cutoffs affect chiral restoration and fluctuations, and for verifying the restoration of thermodynamic consistency as $k\to\infty$. Accordingly, the grand thermodynamic potential of the RG-improved NJL (RGNJL) model can be expressed as

$$\Omega_{\rm RGNJL}=\frac{(M-m)^2}{4G_S}-2N_cN_f\int_0^{\Lambda_0}\frac{d^3p}{(2\pi)^3}E-2N_cN_fT\times\int_0^{\Lambda_T}\frac{d^3p}{(2\pi)^3}\left[\ln\left(1+e^{-\beta(E-\mu)}\right)+\ln\left(1+e^{-\beta(E+\mu)}\right)\right], \tag{7}$$

where $\Lambda_T=k\Lambda_0$ explicitly separates the cutoff scales for the vacuum and thermal contributions.

Although the NJL model successfully describes the chiral phase transition, it does not incorporate confinement dynamics. This limitation motivates its extension to the RG-consistent two-flavor PNJL model. The order parameter for the confinement/deconfinement phase transition is the Polyakov loop,

$$L(\vec{x})=\mathcal{P}\exp\left[i\int_0^{1/T}d\tau A_4(\vec{x},\tau)\right], \tag{8}$$

where A_4 denotes the temporal component of the background gluon field. The traced Polyakov loop and its conjugate are defined as

$$\Phi=\frac{{\rm Tr}_c\,L}{N_c},\quad \bar{\Phi}=\frac{{\rm Tr}_c\,L^\dagger}{N_c}, \tag{9}$$

which effectively serve as imaginary chemical potentials for quarks and can be incorporated into the thermodynamic potential [19, 30–32].

The grand thermodynamic potential of the RGPNJL model can then be written as follows:

$$\begin{aligned}\Omega_{\rm RGPNJL}=&\frac{(M-m)^2}{4G_S}+\mathcal{U}(\Phi,\bar{\Phi},T)-2N_cN_f\int_0^{\Lambda_0}\frac{d^3p}{(2\pi)^3}E\\&-2N_fT\int_0^{\Lambda_T}\frac{d^3p}{(2\pi)^3}\ln(1+3\Phi e^{-\beta(E-\mu)}\\&+3\bar{\Phi}e^{-2\beta(E-\mu)}+e^{-3\beta(E-\mu)})\\&-2N_fT\int_0^{\Lambda_T}\frac{d^3p}{(2\pi)^3}\ln(1+3\bar{\Phi}e^{-\beta(E+\mu)}\\&+3\Phi e^{-2\beta(E+\mu)}+e^{-3\beta(E+\mu)}),\end{aligned} \tag{10}$$

where the same separation of cutoff scales has been applied to the thermal contributions. The effective potential $\mathcal{U}(\Phi,\bar{\Phi},T)$ encodes the gluonic degrees of freedom and cannot be derived directly from QCD. A commonly used phenomenological parametrization is given by [30, 33, 34]

$$\frac{\mathcal{U}(\Phi,\bar{\Phi},T)}{T^4}=-\frac{a(T)}{2}\bar{\Phi}\Phi+b(T)\ln\times\left[1-6\bar{\Phi}\Phi+4(\bar{\Phi}^3+\Phi^3)-3(\bar{\Phi}\Phi)^2\right], \tag{11}$$

where $a(T)=a_0+a_1\left(\frac{T_0}{T}\right)+a_2\left(\frac{T_0}{T}\right)^2$ and $b(T)=b_3\left(\frac{T_0}{T}\right)^3$.

Before solving the RGNJL/RGPNJL models and analyzing the corresponding physical effects, the model parameters must be fixed to reproduce basic hadronic observables in vacuum, such as the pion mass $m_\pi=139.3\,{\rm MeV}$ and the pion decay constant $f_\pi=92\,{\rm MeV}$. In this work, we adopt the standard parameter set $m_u=m_d=5.5\,{\rm MeV}$, $N_c=3$, $N_f=2$, together with $\Lambda_0=651\,{\rm MeV}$ and $G_S=5.04\,{\rm GeV}^{-2}$, which are used consistently in both the RGNJL and RGPNJL models. For the RGPNJL model, the parameters in the Polyakov-loop effective potential are chosen as $a_0=3.51, a_1=-2.47, a_2=15.22, b_3=-1.75$, which are fixed phenomenologically to reproduce lattice QCD results in the pure gauge sector [30, 33, 34].

III. CHIRAL PHASE TRANSITION

The physical constituent quark mass is determined by minimizing the thermodynamic potential. Solving the corresponding gap equation yields the constituent quark mass as a function of temperature and chemical potential for a given RG-modified thermal cutoff, $\Lambda_T=k\Lambda_0$.

For the RGNJL model, the gap equation is given by

$$\frac{\partial\Omega_{\rm RGNJL}}{\partial M}=\frac{M-m}{2G_S}-2N_cN_f\int_0^{\Lambda_0}\frac{d^3p}{(2\pi)^3}\frac{M}{E}+2N_cN_f\times\int_0^{\Lambda_T}\frac{d^3p}{(2\pi)^3}\frac{M}{E}\left[\frac{1}{1+e^{\beta(E-\mu)}}+\frac{1}{1+e^{\beta(E+\mu)}}\right]=0. \tag{12}$$

Similarly, in the RGPNJL model, the stationarity conditions with respect to M, Φ, and $\bar{\Phi}$ yield a coupled set of gap equations. The gap equation for the constituent quark mass is given by

CPC Accepted

$$\frac{\partial\Omega_{\rm RGPNJL}}{\partial M}=\frac{M-m}{2G_S}-2N_cN_f\int_0^{\Lambda_0}\frac{d^3p}{(2\pi)^3}\frac{M}{E}+2N_f\int_0^{\Lambda_T}\frac{d^3p}{(2\pi)^3}\frac{M}{E}\frac{3\Phi e^{-\beta(E-\mu)}+6\bar{\Phi}e^{-2\beta(E-\mu)}+3e^{-3\beta(E-\mu)}}{1+3\Phi e^{-\beta(E-\mu)}+3\bar{\Phi}e^{-2\beta(E-\mu)}+e^{-3\beta(E-\mu)}}$$
$$+2N_f\int_0^{\Lambda_T}\frac{d^3p}{(2\pi)^3}\frac{M}{E}\frac{3\bar{\Phi}e^{-\beta(E+\mu)}+6\Phi e^{-2\beta(E+\mu)}+3e^{-3\beta(E+\mu)}}{1+3\bar{\Phi}e^{-\beta(E+\mu)}+3\Phi e^{-2\beta(E+\mu)}+e^{-3\beta(E+\mu)}}=0. \tag{13}$$

The stationarity conditions for the Polyakov loop variables Φ and $\bar{\Phi}$ are given by

$$\frac{\partial\Omega_{\rm RGPNJL}}{\partial\Phi}=T^4\left[-\frac{a(T)}{2}\bar{\Phi}+b(T)\frac{-6\bar{\Phi}+12\Phi^2-6\bar{\Phi}^2\Phi}{1-6\bar{\Phi}\Phi+4\left(\bar{\Phi}^3+\Phi^3\right)-3(\bar{\Phi}\Phi)^2}\right]-2N_fT\int_0^{\Lambda_T}\frac{d^3p}{(2\pi)^3}\frac{3e^{-\beta(E-\mu)}}{1+3\Phi e^{-\beta(E-\mu)}+3\bar{\Phi}e^{-2\beta(E-\mu)}+e^{-3\beta(E-\mu)}}$$
$$-2N_fT\int_0^{\Lambda_T}\frac{d^3p}{(2\pi)^3}\frac{3e^{-\beta(E+\mu)}}{1+3\Phi e^{-\beta(E+\mu)}+3\bar{\Phi}e^{-2\beta(E+\mu)}+e^{-3\beta(E+\mu)}}=0, \tag{14}$$

$$\frac{\partial\Omega_{\rm RGPNJL}}{\partial\bar{\Phi}}=T^4\left[-\frac{a(T)}{2}\Phi+b(T)\frac{-6\Phi+12\bar{\Phi}^2-6\bar{\Phi}\Phi^2}{1-6\bar{\Phi}\Phi+4\left(\bar{\Phi}^3+\Phi^3\right)-3(\bar{\Phi}\Phi)^2}\right]-2N_fT\int_0^{\Lambda_T}\frac{d^3p}{(2\pi)^3}\frac{3e^{-2\beta(E-\mu)}}{1+3\Phi e^{-\beta(E-\mu)}+3\bar{\Phi}e^{-2\beta(E-\mu)}+e^{-3\beta(E-\mu)}}$$
$$-2N_fT\int_0^{\Lambda_T}\frac{d^3p}{(2\pi)^3}\frac{3e^{-2\beta(E+\mu)}}{1+3\Phi e^{-\beta(E+\mu)}+3\bar{\Phi}e^{-2\beta(E+\mu)}+e^{-3\beta(E+\mu)}}=0. \tag{15}$$

By solving the gap equations of the NJL/PNJL models numerically, the constituent quark mass is obtained as a function of temperature and chemical potential for different values of the thermal cutoff Λ_T. The corresponding results for the NJL and PNJL models are shown in Fig. 1 and Fig. 2, respectively. The critical temperature of the chiral phase transition, T_c, can be defined by the condition

$$T_c:\quad \left|\frac{dM}{dT}\right|_{T=T_c}=\max\left|\frac{dM}{dT}\right|, \tag{16}$$

which characterizes the location at which the constituent quark mass changes most rapidly.

As shown in Fig. 1 and Fig. 2, the NJL and PNJL models exhibit similar qualitative behavior. In the low-temperature regime, the constituent quark mass remains nearly constant and depends only weakly on the choice of Λ_T. This reflects the dominance of the vacuum contribution, for which thermal effects are negligible. As the temperature approaches the transition region, however, the dependence on Λ_T becomes pronounced. Larger values of Λ_T lead to an earlier and more rapid decrease in the constituent quark mass, corresponding to a lower pseudocritical temperature T_c. This behavior indicates that increasing the thermal cutoff effectively enhances the contribution of high-momentum thermal modes, thereby accelerating the restoration of chiral symmetry.

A more detailed inspection of the figures reveals an additional feature. For the case $k=1.0$, corresponding to $\Lambda_T=\Lambda_0$, the constituent quark mass decreases with increasing temperature but remains above the current quark mass m even at high temperature. In contrast, for larger values of k, the constituent quark mass can fall below the current quark mass in the high-temperature regime. This behavior is unphysical, because the current quark mass sets the lower bound for the dynamical mass in the chirally restored phase.

Beyond the temperature-dependent mass evolution, the structure of the chiral phase boundary, characterized by the critical temperature T_c as a function of the baryon chemical potential $\mu_B=3\mu$, provides further insight into the framework. As illustrated in Fig. 3, both the RGNJL (a) and RGPNJL (b) models exhibit a monotonically decreasing phase boundary as the chemical potential increases. Notably, increasing the parameter k systematically suppresses T_c across the entire range of μ_B. However, this suppression is more pronounced at low chemical potentials; as μ_B approaches 1000 MeV, the curves for different values of k tend to converge, suggesting that the sensitivity of the chiral transition temperature to the RG-consistent modification diminishes at high baryon densities.

Therefore, although the RG-consistent extension modifies the thermal contributions and shifts the chiral transition, it does not fully eliminate the artifacts associated with the cutoff prescription. In particular, the appearance of $M<m$ at large k suggests that the RGNJL/RGPNJL framework still requires further refinement to achieve a fully consistent description of the high-temperature regime.

CPC Accepted

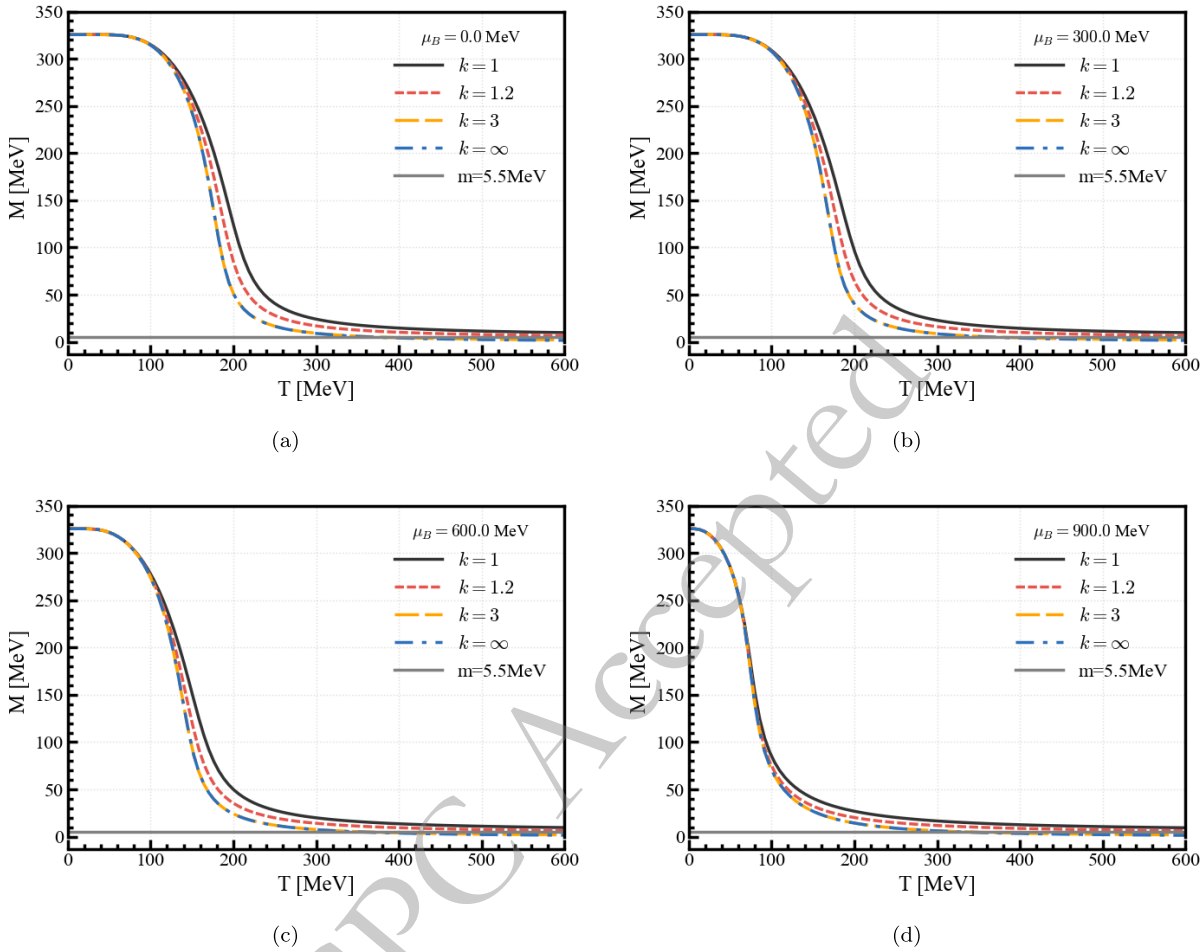


Fig. 1. (color online) Constituent quark mass M as a function of temperature T for several truncation factors k (i.e., $\Lambda_T = k\Lambda_0$) at fixed values of the baryon chemical potential, $\mu_B = 0$, 300, 600, and 900 MeV, in the RGNJL model.

CPC Accepted

IV. THERMODYNAMIC QUANTITIES AND BARYON NUMBER FLUCTUATIONS

In addition to the chiral phase transition and the behavior of the constituent quark mass, it is instructive to analyze thermodynamic observables that can be derived directly from the grand potential. These quantities provide complementary information about the equation of state and the response of the system to thermal excitations, and are therefore essential for a comprehensive understanding of the QCD medium [35–37].

The pressure is defined as the negative of the grand potential density, $P = -\Omega$. To ensure a physically meaningful normalization, the vacuum contribution is subtracted so that the pressure vanishes at zero temperature and chemical potential. Accordingly, the pressure is given by

$$P(\mu, T) = \Omega(0,0) - \Omega(\mu, T), \tag{17}$$

where $\Omega(0,0)$ denotes the grand potential in the vacuum.

The energy density ϵ can be obtained using standard thermodynamic relations,

$$\epsilon = -T^2 \frac{\partial(\Omega/T)}{\partial T}\bigg|_V = -T\frac{\partial\Omega}{\partial T}\bigg|_V + \Omega - \Omega(0,0), \tag{18}$$

This expression explicitly incorporates the vacuum subtraction, ensuring consistency with the pressure normalization.

The specific heat at constant volume, which characterizes the system's response to changes in temperature, is defined as

$$C_V = \frac{\partial\epsilon}{\partial T}\bigg|_V = -T\frac{\partial^2\Omega}{\partial T^2}\bigg|_V. \tag{19}$$

This quantity is particularly sensitive to the chiral phase transition and typically exhibits a peak near the pseudo-critical temperature.

Another important observable is the squared speed of sound, which characterizes the stiffness of the equation of state and plays a crucial role in the hydrodynamic evolu-

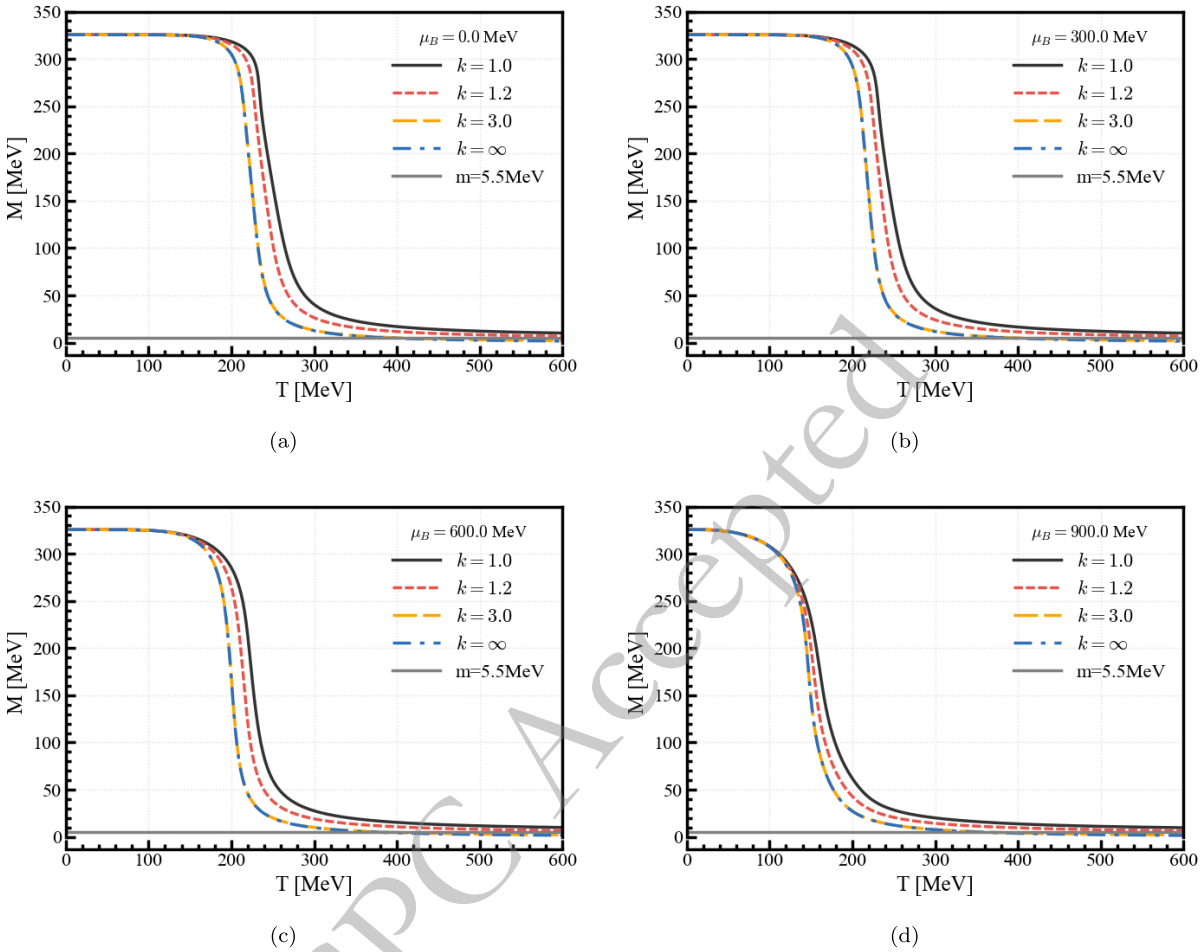


Fig. 2. (color online) The constituent quark mass M as a function of temperature T for different truncation factors k (i.e., $\Lambda_T = k\Lambda_0$) at fixed values of the baryon chemical potential in the RGPNJL model, illustrating the influence of confinement effects.

CPC Accepted

tion of the medium. At constant entropy, it is given by

$$v_s^2 = \left.\frac{\partial P}{\partial \epsilon}\right|_S = \left.\frac{\partial \Omega}{\partial T}\right|_V \Big/ T\left.\frac{\partial^2 \Omega}{\partial T^2}\right|_V . \tag{20}$$

These thermodynamic quantities serve as independent probes for assessing the impact of RG-consistent modifications on the equation of state and for evaluating the validity of the RGNJL and RGPNJL frameworks. As illustrated in Fig. 4 and Fig. 5, both models exhibit a systematic increase in the scaled pressure (P/T^4), energy density (ϵ/T^4), and specific heat (C_V/T^3) in the high-temperature regime as the parameter k increases, eventually approaching a stable plateau. This behavior is consistent with theoretical expectations: at high temperatures, the coupling becomes weak, and the thermal quantities converge toward the Stefan-Boltzmann limit of an ideal, free Fermi gas.

However, comparison of the two models reveals clear differences in the transition dynamics. In the RGNJL model (Fig. 4a-c), the thermodynamic quantities increase relatively smoothly and gradually with T/T_c. In contrast, the RGPNJL model (Fig. 5a-c) exhibits substantially steeper growth, particularly in the range $0.8 \leq T/T_c \leq 1.2$. The specific heat C_V/T^3 in Fig. 5c shows a sharp, pronounced peak near the pseudo-critical temperature T_c, which is notably stronger than the broader, more muted peak observed in the RGNJL model (Fig. 4c). This indicates that the inclusion of the Polyakov loop potential in the RGPNJL framework more effectively simulates the rapid change in degrees of freedom associated with the confinement-deconfinement transition.

The behavior of the squared speed of sound (v_s^2) presents a more complex scenario, with distinct implications for causality and conformality. In the RGNJL model (Fig. 4d), the baseline case with equal cutoffs ($k = 1.0$) shows an unphysical violation of causality, with $v_s^2 > 1$ at high temperatures, due to the severe truncation of thermal phase space. Enforcing the unregularized thermal limit ($k \to \infty$) successfully constrains v_s^2 to the conformal limit of 1/3, thereby resolving the causality violation and restoring thermodynamic consistency.

The RGPNJL model (Fig. 5d) exhibits a more intric-

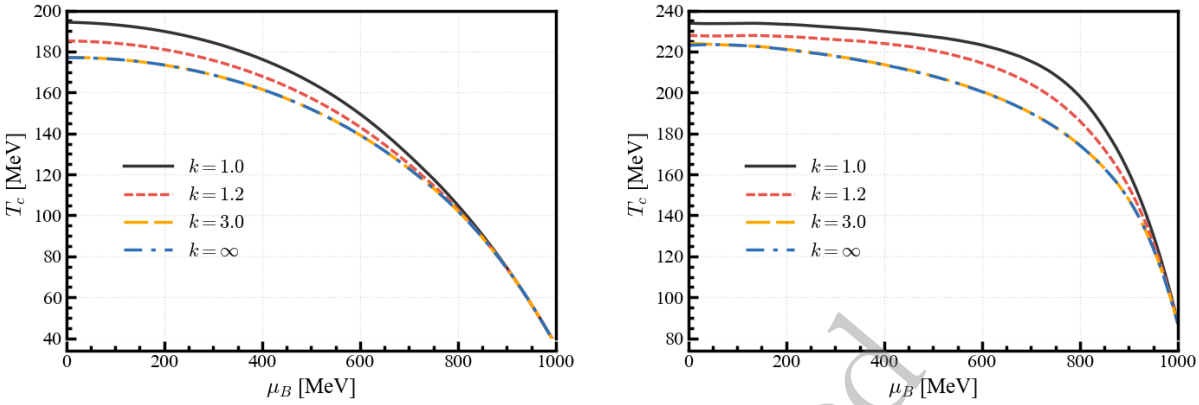


Fig. 3. (color online) Critical temperature T_c of the chiral phase transition as a function of the baryon chemical potential μ_B for the RGNJL (a) and RGPNJL (b) models at different values of k.

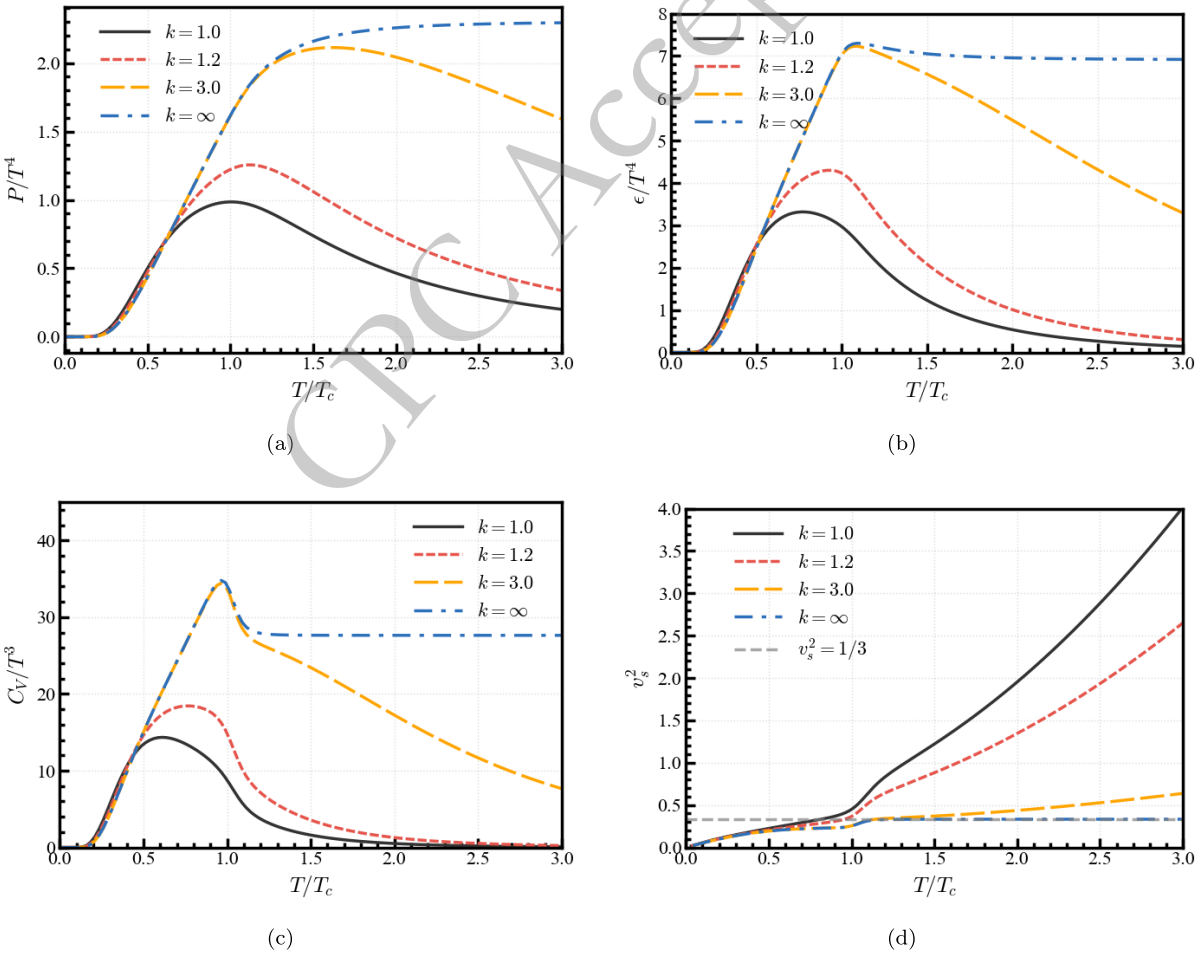


Fig. 4. (color online) Thermodynamic quantities as functions of temperature at zero chemical potential for the RGNJL model.

ate, non-monotonic dependence on k. Although both small ($k \approx 1$) and very large ($k \to \infty$) values of k respect the conformal limit, intermediate values, most notably $k \approx 3.0$, show the speed of sound rising above the conformal limit ($v_s^2 > 1/3$) for temperatures $T/T_c > 1.5$.

This non-monotonic behavior highlights a non-trivial dynamical interplay between the Polyakov loop potential and high-momentum quark modes. At low truncation factors ($k \sim 1$), the Polyakov-loop background fields $(\Phi, \bar{\Phi})$ suppress thermal quark excitations through statist-

CPC Accepted

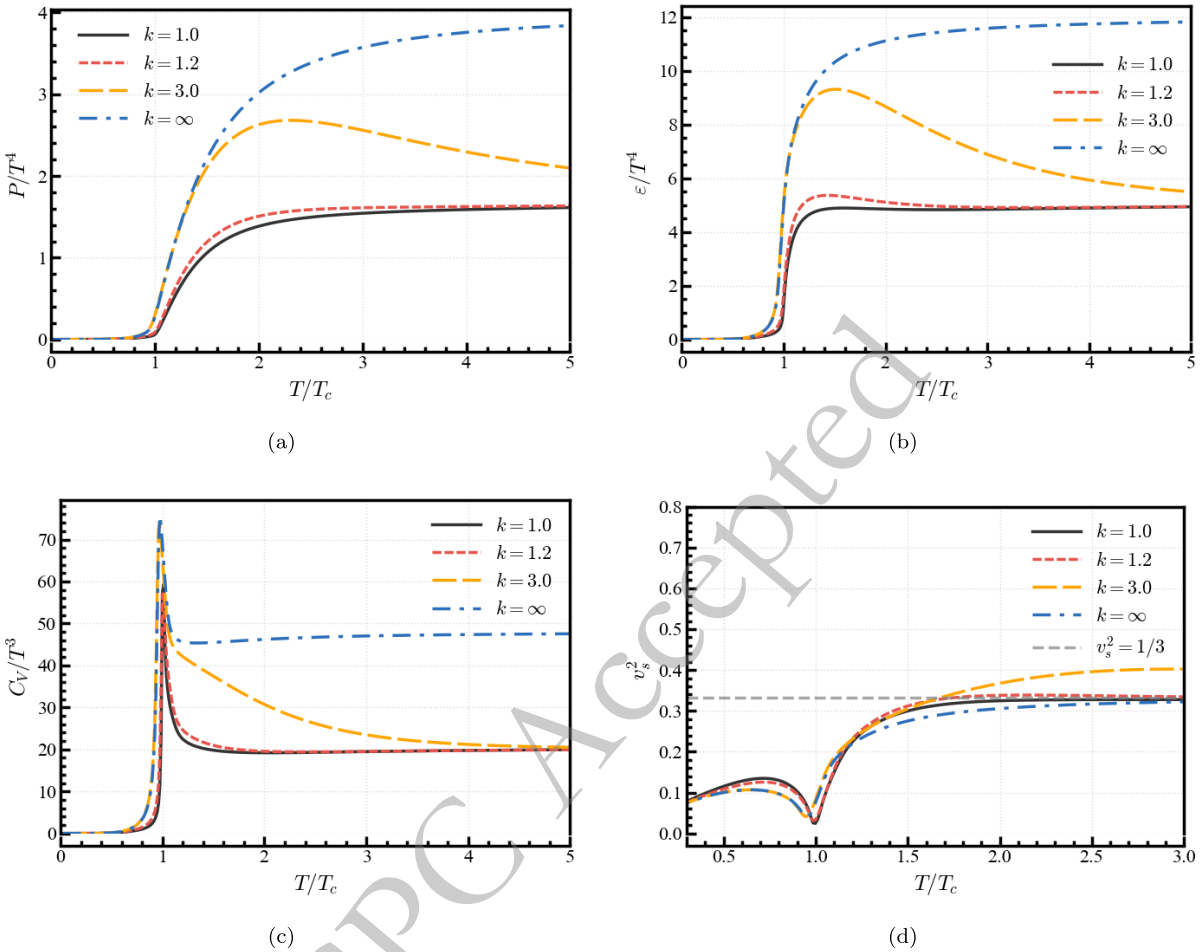


Fig. 5. (color online) Thermodynamic quantities as functions of temperature at zero chemical potential in the RGPNJL model.

CPC Accepted

ical confinement, acting as an effective dynamical regulator that maintains $v_s^2 \leq 1/3$ and $M \geq m$ even when momentum space is artificially restricted. However, this feature should not be misinterpreted as implying that $k \sim 1$ represents an optimal physical parameter choice. At asymptotically high temperatures, the system must recover the Stefan-Boltzmann limit of free quarks and gluons, which strictly requires taking $k \to \infty$. The transient overshoot of the conformal limit observed at intermediate $k \approx 3$ indicates an intrinsic tension between the phenomenological Polyakov-loop potential, parameterized using pure-gauge lattice data, and the quark momentum integration boundary. This underscores the need to systematically explore the truncation scale k as a diagnostic tool rather than treating it as an adjustable free parameter.

As a complement to the thermodynamic analysis above, the nature of the chiral phase transition can be further elucidated by examining higher-order fluctuations of the net-baryon number. These fluctuations are characterized by generalized susceptibilities, χ_n^B, which are derived from the thermodynamic potential Ω (where $P = -\Omega$):

$$\chi_n^B = \frac{\partial^n [P/T^4]}{\partial [\mu_B/T]^n}. \tag{21}$$

The corresponding cumulants of the baryon-number distributions, C_n^B, can then be expressed as follows:

$$C_n^B = VT^3 \chi_n^B. \tag{22}$$

Defining the variance $\sigma^2 = C_2^B$ and the kurtosis $\kappa = C_4^B/(\sigma^2)^2$ allows one to construct the ratio $\kappa\sigma^2$, which provides an important link between predictions from theoretical frameworks and experimental observables:

$$\kappa\sigma^2 = \frac{C_4^B}{C_2^B} = \frac{\chi_4^B}{\chi_2^B}. \tag{23}$$

This ratio, $\kappa\sigma^2$, is a highly sensitive indicator of the criticality of the QCD phase transition [39–41]. These ratios enable a rigorous quantitative comparison between the RGNJL/RGPNJL frameworks and lattice QCD data, providing an essential benchmark for determining whether the RG-consistent modifications accurately capture the

fluctuation properties of the hot, dense medium.

As illustrated in Figs. 6 and 7, the behavior of the net-baryon number kurtosis $\kappa\sigma^2$ exhibits distinct characteristics depending on the model and chemical potential. At vanishing chemical potential ($\mu_B = 0$), the kurtosis in both models remains relatively stable in the low-temperature regime, consistent with the Hadron Resonance Gas (HRG) limit, where $\kappa\sigma^2 \approx 1$. As the temperature increases, the RGNJL model (Fig. 6(a)) shows minimal sensitivity to the RG parameter k and substantially underestimates the lattice simulation data in the transition region. In contrast, the RGPNJL model (Fig. 7(a)) provides a much better qualitative match to the lattice results. In particular, as the RG consistency condition is approached ($k \to \infty$), the kurtosis in the RGPNJL model decreases more rapidly for $T/T_c \geq 1.1$, closely following the lattice trend as it approaches the ideal free quark gas (FQG) limit of approximately 0.068.

However, as the chemical potential μ_B increases, the kurtosis develops a pronounced, non-monotonic dependence on both temperature and the parameter k. In the range $0.8 \leq T/T_c \leq 1.2$, the fluctuations become increasingly volatile: larger values of k lead to a higher maximum and a deeper minimum in the kurtosis. Interestingly, increasing μ_B shifts the peak position of the kurtosis toward lower temperatures, a feature observed in both models but substantially amplified in the RGPNJL framework (Figs. 7(c) and 7(d)). While the RGNJL model (Fig. 6) maintains relatively smooth oscillations even at high μ_B, the RGPNJL model displays increasingly sharp, spike-like structures. For $\mu_B = 600$ MeV, the RGPNJL model with $k \to \infty$ exhibits a sharp oscillation from a positive peak near $\kappa\sigma^2 \approx 4$ to a negative dip below -6. This pronounced intensification of the extrema near $T/T_c \approx 1.0$ suggests that the coupling between the Polyakov loop and the RG-consistent chiral dynamics enhances the model's sensitivity to proximity to the critical point at high baryon density. These shifts indicate that al-

CPC Accepted

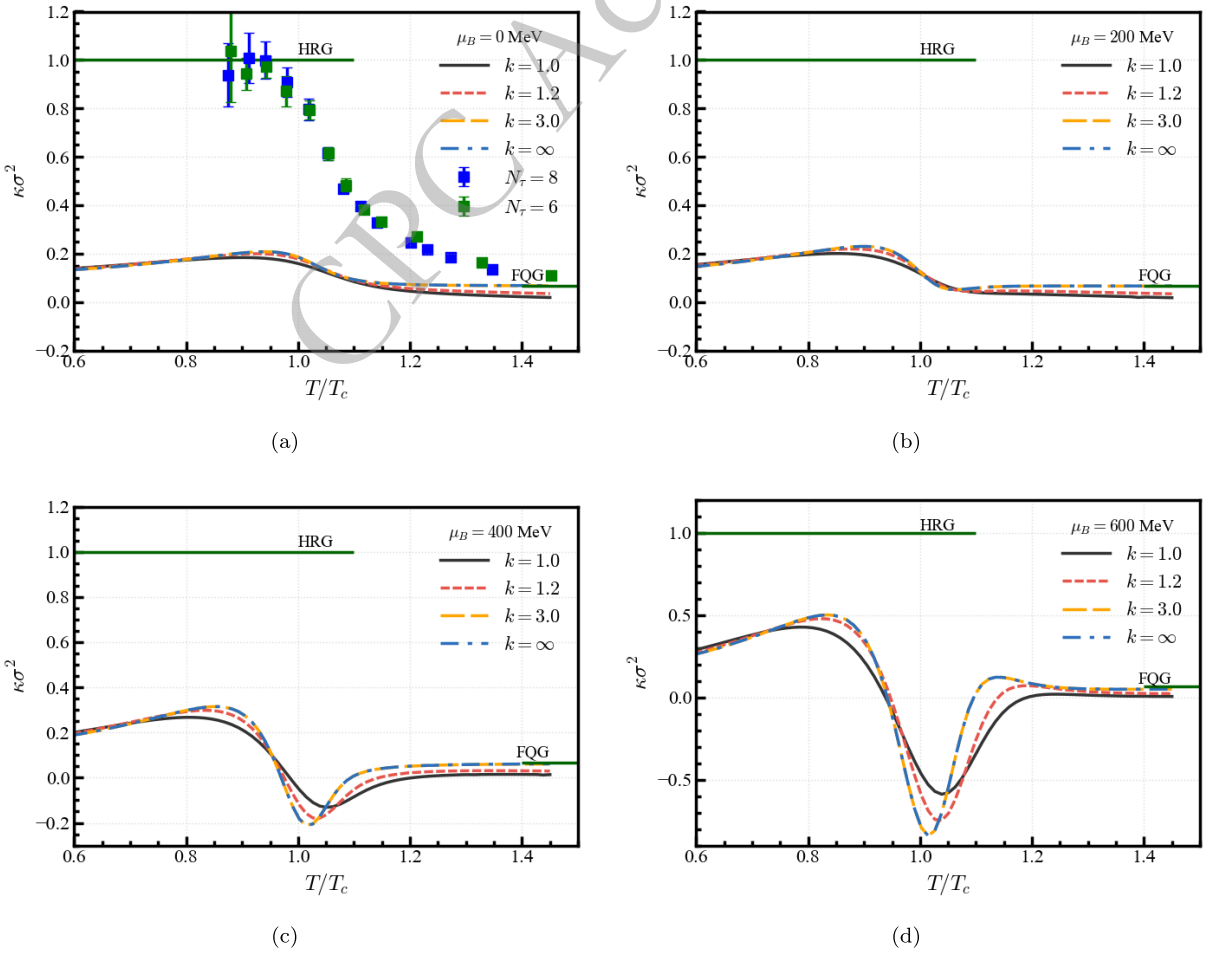


Fig. 6. (color online) The net-baryon number kurtosis $\kappa\sigma^2$ is shown as a function of temperature T/T_c for various truncation factors k (where $\Lambda_T = k\Lambda_0$) at fixed baryon chemical potentials $\mu_B = 0, 200, 400$, and 600 MeV in the RGNJL model. The results for $\mu_B = 0$ are compared with lattice QCD data from [38]. The horizontal lines indicate the hadron resonance gas (HRG) limit ($\kappa\sigma^2 = 1$) and the ideal free-quark gas (FQG) limit ($\kappa\sigma^2 = 0.068$).

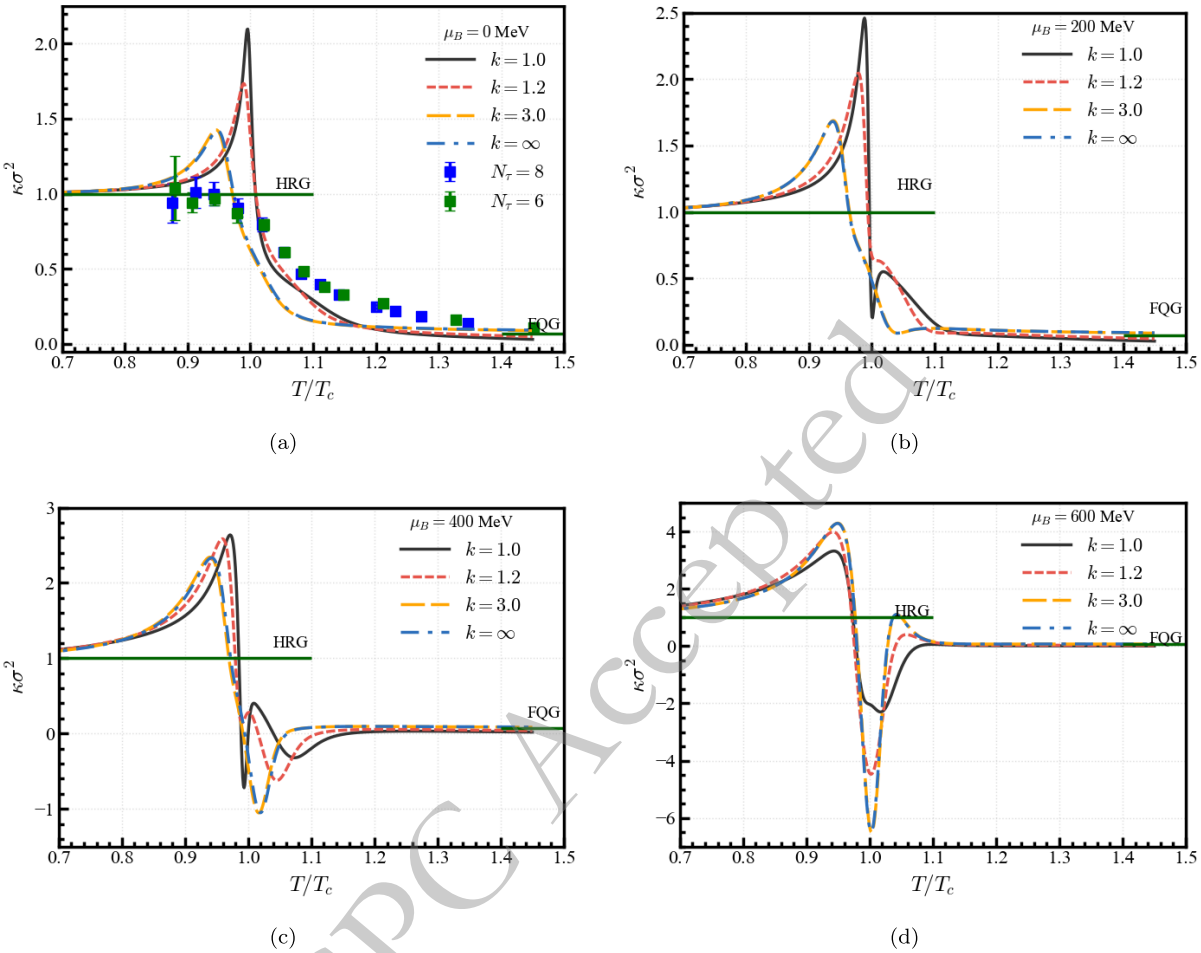


Fig. 7. (color online) The net-baryon-number kurtosis $\kappa\sigma^2$ is shown as a function of the temperature T/T_c for various truncation factors k (where $\Lambda_T = k\Lambda_0$) at fixed baryon chemical potentials $\mu_B = 0, 200, 400,$ and 600 MeV in the RGPNJL model. The results at $\mu_B = 0$ are compared with lattice QCD data from [38]. The horizontal lines indicate the hadron resonance gas (HRG) limit ($\kappa\sigma^2 = 1$) and the ideal free quark gas (FQG) limit ($\kappa\sigma^2 = 0.068$).

though RG consistency improves high-temperature thermodynamics, it simultaneously amplifies the signatures of critical fluctuations in the dense medium.

V. CONCLUSION AND DISCUSSION

In this study, we systematically investigated the effects of thermal cutoff modifications on thermodynamic properties, chiral phase transitions, and net-baryon number fluctuations within the NJL and PNJL frameworks from the perspective of renormalization group (RG) consistency. Our results demonstrate that extending the thermal cutoff scale $\Lambda_T = k\Lambda_0$ significantly modifies the behavior of the constituent quark mass, the critical temperature T_c, and higher-order baryon number fluctuations. As the truncation factor increases toward $k \to \infty$, both models successfully converge to the expected Stefan-Boltzmann limits at high temperatures, addressing a longstanding limitation of fixed-cutoff effective theories. This convergence confirms that the unregularized thermal limit ($k \to \infty$) provides a reliable method for incorporating high-momentum thermal excitations above the Matsubara scale ($\Lambda \geq \pi T$), thereby partially restoring RG consistency.

A comparative analysis of the NJL and PNJL models reveals distinct advantages as well as subtle interplay with confinement dynamics. In the NJL model, enforcing the unregularized thermal limit ($k \to \infty$) effectively resolves the unphysical causality violation ($v_s^2 > 1$) present in the standard equal-cutoff ($k = 1$) baseline, constraining the speed of sound to the conformal limit 1/3. Furthermore, the PNJL model exhibits superior agreement with lattice QCD data for net-baryon number kurtosis at vanishing chemical potential, particularly in capturing the rapid crossover transition near T_c. However, a notable artifact persists in both models at large truncation scales ($k \to \infty$): the constituent quark mass can decrease slightly below the current quark mass ($M < m$) in the high-temperature restored phase. This suggests that, although extending the thermal integration accounts for high-mo-

CPC Accepted

mentum thermal modes, the matching between vacuum and thermal regulators requires further refinement to strictly preserve the dynamical lower bound of the constituent mass.

Furthermore, the behavior of the speed of sound and the kurtosis extrema in the PNJL model indicates a nontrivial competition between chiral dynamics and the Polyakov-loop potential. We observed that intermediate values of k (e.g., $k \approx 3.0$) can cause v_s^2 to exceed the conformal limit in the PNJL framework, a feature absent in the NJL case. This nonmonotonic sensitivity does not imply that $k \sim 1$ should be selected as an optimal free parameter. Rather, it highlights that the Polyakov loop dynamically suppresses quark excitations at low temperatures through statistical confinement, temporarily mitigating truncation artifacts in the confined phase. At higher temperatures, however, thermodynamic consistency fundamentally requires $k \to \infty$ to capture all active thermal modes. In dense matter ($\mu_B > 400$ MeV), the unregularized thermal modifications substantially amplify the magnitude of kurtosis oscillations near the phase transition, underscoring the heightened sensitivity of critical fluctuation observables to high-momentum thermal phase space in dense matter.

In conclusion, the scan of the thermal cutoff from $k = 1$ to $k \to \infty$ serves as an essential diagnostic tool for NJL-type models by clarifying how high-momentum thermal modes systematically influence chiral restoration and fluctuations. Rather than introducing k as an adjustable free parameter, our analysis demonstrates that $k \to \infty$ is the required physical limit for restoring Stefan-Boltzmann scaling, while intermediate variations elucidate the intricate coupling between confinement dynamics and thermal integration boundaries. Future work should focus on formulating a fully self-consistent functional RG flow that incorporates running bare parameters in the presence of Polyakov loops, as well as on extending this framework to the $(2+1)$-flavor case to incorporate the effects of strangeness on the QCD phase diagram.

CPC Accepted

References

[1] Kenji Fukushima and Tetsuo Hatsuda, Rept. Prog. Phys. **74**, 014001 (2011)
[2] Larry McLerran and Robert D. Pisarski, Nucl. Phys. A **796**, 83 (2007)
[3] A. Bazavov *et al*., Phys. Rev. D **85**, 054503 (2012)
[4] Misha A. Stephanov, K. Rajagopal, and Edward V. Shuryak, Phys. Rev. Lett. **81**, 4816 (1998)
[5] Z. Fodor and S. D. Katz, JHEP **04**, 050 (2004)
[6] Misha A. Stephanov, K. Rajagopal, and Edward V. Shuryak, Phys. Rev. D **60**, 114028 (1999)
[7] B. Friman, F. Karsch, K. Redlich, and V. Skokov, Eur. Phys. J. C **71**, 1694 (2011)
[8] L. Adamczyk *et al*., Phys. Rev. Lett. **112**, 032302 (2014)
[9] M. M. Aggarwal *et al*. An Experimental Exploration of the QCD Phase Diagram: The Search for the Critical Point and the Onset of De-confinement. 7 2010.
[10] J. Adam *et al*. *Phys. Rev. Lett.*, 126(9): 092301, 2021.[Erratum: Phys.Rev.Lett. 134, 139902 (2025)].
[11] B. E. Aboona *et al*., Phys. Rev. Lett. **135**(14), 142301 (2025)
[12] Yoichiro Nambu and G. Jona-Lasinio, Phys. Rev. **122**, 345 (1961)
[13] Yoichiro Nambu and G. Jona-Lasinio, Phys. Rev. **124**, 246 (1961)
[14] S. P. Klevansky, Rev. Mod. Phys. **64**, 649 (1992)
[15] Michael Buballa, Phys. Rept. **407**, 205 (2005)
[16] Shijun Mao, Phys. Rev. D **110**(5), 054002 (2024)
[17] Jie Mei, Rui Wen, Shijun Mao, Mei Huang, and Kun Xu, Phys. Rev. D **110**(3), 034024 (2024)
[18] Mei Huang and Pengfei Zhuang, Symmetry **15**(2), 541 (2023)
[19] Kenji Fukushima, Phys. Lett. B **591**, 277 (2004)
[20] Kenji Fukushima. *Phys. Rev. D*, 77: 114028, 2008.[Erratum: Phys.Rev.D 78, 039902 (2008)].
[21] Claudia Ratti, Michael A. Thaler, and Wolfram Weise. Phase diagram and thermodynamics of the PNJL model. 4 2006.
[22] Lang Yu, Hao Liu, and Mei Huang, Phys. Rev. D **94**(1), 014026 (2016)
[23] Kai Xue, Xiaozhu Yu, and Xinyang Wang, Chin. Phys. C **46**(5), 013103 (2022)
[24] Sidney S. Avancini, Ricardo L. S. Farias, Norberto N. Scoccola, and William R. Tavares, Phys. Rev. D **99**(11), 116002 (2019)
[25] Sidney S. Avancini, Ricardo L. S. Farias, and William R. Tavares, Phys. Rev. D **99**(5), 056009 (2019)
[26] Christof Wetterich, Phys. Lett. B **301**, 90 (1993)
[27] Jens Braun, Marc Leonhardt, and Jan M. Pawlowski, SciPost Phys. **6**(5), 056 (2019)
[28] Hosein Gholami, Marco Hofmann, and Michael Buballa, Phys. Rev. D **111**(1), 014006 (2025)
[29] Fan Lin, Kun Xu, and Mei Huang, Phys. Rev. D **106**(1), 016005 (2022)
[30] Nathan Weiss, Phys. Rev. D **24**, 475 (1981)
[31] Nathan Weiss, Phys. Rev. D **25**, 2667 (1982)
[32] Kenji Fukushima and Koichi Ohta, J. Phys. G **26**, 1397 (2000)
[33] C. Ratti, Simon Roessner, M. A. Thaler, and W. Weise, Eur. Phys. J. C **49**, 213 (2007)
[34] Guo-yun Shao, Zhan-duo Tang, Xue-yan Gao, and Wei-bo He, Eur. Phys. J. C **78**(2), 138 (2018)
[35] Claudia Ratti and Wolfram Weise, Phys. Rev. D **70**, 054013 (2004)
[36] Jin-Li Zhang, Cheng-Ming Li, and Hong-Shi Zong, Chin. Phys. C **42**(12), 123105 (2018)
[37] Sanjay K. Ghosh, Tamal K. Mukherjee, Munshi G. Mustafa, and Rajarshi Ray, Phys. Rev. D **73**, 114007 (2006)
[38] A. Bazavov *et al*., Phys. Rev. D **95**(5), 054504 (2017)
[39] Wei-jie Fu, Xiaofeng Luo, Jan M. Pawlowski, Fabian Rennecke, Rui Wen, and Shi Yin, Phys. Rev. D **104**(9), 094047 (2021)
[40] Wei-jie Fu, Xiaofeng Luo, Jan M. Pawlowski, Fabian Rennecke, Rui Wen, and Shi Yin, PoS **CPOD2021**, 009 (2022)
[41] Yi Lu, Fei Gao, Xiaofeng Luo, Lei Chang, and Yuxin Liu, Sci. China Phys. Mech. Astron. **68**(5), 251012 (2025)